Journal of Telecommunication, Electronic and Computer Engineering
ISSN: 2180 – 1843 e-ISSN: 2289-8131 Vol. 18 No. 1 (2026) 19-27
jtec.utem.edu.my
DOI: https://doi.org/10.54554/jtec.2026.18.01.003

360° Scanning of Stationary Objects inside Room With a 24 GHz Commercial RADAR Module

Shalini Kashyap, Amit Birwal and Kamlesh Patel*
Department of Electronic Science, University of Delhi South Campus, New Delhi,110021, India.

Article Info
Article history:
Received Sep 22th, 2025
Revised Mar 11th, 2026
Accepted Mar 30th, 2026
Published Mar 31st, 2026

Index Terms:
RADAR
FFT
MATLAB
FMCW
Heatmap
Range resolution
RMSE

Abstract
In this work, various stationary objects were detected within a room measuring 4.88 × 3.91 m². The data were captured by a 24 GHz commercial radar module, OPS243-C. The experiments were performed in two scenarios: over each wall or at different angles of the radar positions, and, secondly, by mounting this radar module on a rotating motor to scan each object over a 360° coverage. In addition, to suppress background noise and filter out strong signals in the heatmap results, a noise threshold and a Gaussian smoothing filter were applied. The predicted distances of objects were then obtained by applying suitable curve-fitting models to radar data captured in each scenario. The corresponding images captured in each scenario were used to validate the 2D and 3D heatmaps for object distances after curve fitting. Thus, for each wall scan, a linear curve-fitting model was found to be sufficient, whereas for entire-room scanning, a 6th-order polynomial curve-fitting model was found to provide the best predicted distances by the module. The methodology discussed in this work is useful for analyzing field-grown crops and continuously monitoring their health.

*Corresponding Author: kpatel@south.du.ac.in

I. INTRODUCTION

In recent years, radar has extended its applications beyond the military and defense domains to social, medical, and commercial sectors. Primarily, it is used for object speed and direction detection (angle-based), and range estimation. More recently, radar applications have been explored for health monitoring of humans, animals, and crops. Here, the objects belong to various categories with different compositions, including living and non-living bodies. In these radars, the reflected waves carry information about these objects beyond traditional electronic warfare applications. The velocity of objects such as a swinging conducting ball, a man walking and running, and a car, is estimated using a 5.8 GHz radar system in [1]. A millimeter-wave 24 GHz radar captures the breathing and heart rates of a human in [2]. In [3], the estimation of soil water content is performed using a 24 GHz radar system with a bandwidth of 200 MHz. In [4], a frequency-modulated continuous wave (FMCW) radar is used to collect real-time traffic information. In [5], leaf withering conditions are monitored online using a 60 GHz radar, whereas in [6], the 60 GHz signal is used to detect vehicle occupancy, leveraging the advantages of FMCW and a multiple-input multiple-output (MIMO) architecture by extracting a feature matrix from 2D imaging. In [7], a car tracking and detection system is reported to measure the range and speed of cars at 77 GHz using a range-Doppler map and a 2D constant false alarm rate (CFAR) algorithm. In recent years, many radars operating at frequencies from 2.4 GHz to 77 GHz have been developed and reported.

To develop a compact radar for commercial applications, a radar sensor module (with FMCW, Doppler, or Pulse operation) is required to transmit and receive radio-frequency signals at 24 GHz, 60 GHz, or 77 GHz, and to collect raw information about the objects. To process captured data, data acquisition, control, and signal processing systems are required, such as a microcontroller or a digital signal processing system to interface with the radar sensor. A battery-powered power supply is also required to power the handheld radar, including the module and signal processing unit. Antennas with wide beamwidths or high directivity are integrated with or placed externally to the radar module. Lastly, a wireless interface, e.g., Bluetooth/Wi-Fi, is used to display on a mobile app or personal computer.

Consequently, many works on a commercial radar module, the OPS243 series, have recently been reported, as it supports both FMCW and Doppler modes. Small displacements can be detected with high resolution for non-contact vital signs in real time based on phase differences with an estimation of range accuracy less than 4.5 m using a 24 GHz FMCW radar

[8], In [9], the FMCW radar model, OPS241-B is used for patient respiratory data analysis and its integration into the Internet of Things using an MQTT server and Raspberry Pi 4. In another work, a 24 GHz radar system is integrated with the mini-PC to detect vital sign patterns behind the wall by eliminating the beat frequency [10], where the phase detection method is used to extract the Doppler response behind a concrete brick of thickness 20-40 cm, with an error rate of 3.375 cm. In [11], the OPS243-C radar model is used to detect sneezing, coughing, face touching, and entry and exit activities in a smart home application. In [12], three Doppler-based radar models are used to estimate the velocity of single and multiple moving objects in various indoor and outdoor scenes, while eight types of medication tampering activities are monitored with the OPS243 model in [13]. The breathing of humans under rubble, i.e., in through-the-wall condition, is detected by extracting the Doppler response using a phase-detection method in a 24 GHz radar system [14].

Recently, many radar-based works have been reported for indoor scanning applications. For example, in [15] researchers use a 24 GHz radar with wavelet decomposition, clustering and tracking approaches to count people in indoor environment, whereas in [16], the 24 GHz radar combined with the Convolutional Neural Network (CNN) deep learning is used to localize humans, which requires high training datasets and increases computational complexity. In [17], a neural network architecture is proposed for non-line-of-sight (NLOS) and line-of-sight (LOS) object tracking using mmWave radar. In [18], a 62 GHz FMCW MIMO antenna radar system uses a 2D range-mapping technique to estimate indoor environment. Additionally, many radars operating at 24 GHz have been reported for multiple target detection in various applications, such as boats and life jackets [19], detection of small drones and humans [20], static object detection and estimation of water velocity [21], radial speed measurement of pedestrians, cars, trucks, and motorcycles [22], human movement analysis for 3D security imaging [23], differentiation between real humans and human-mimicking objects [24], victim localization under rubble using unmanned aerial vehicles (UAV) [25], and target detection and tracking combined with infrared thermal detection systems [26], as well as plant population estimation [27].

The accuracy of such a radar sensor depends on various parameters, such as range resolution, speed resolution, signal-to-noise ratio (SNR), interference with other co-frequencies, narrow beam angle, and a higher field of view (FoV). The validation of a newly developed radar sensor is typically performed by comparing its data with actual range and speed measurements, i.e., by placing objects at a fixed distances and moving objects at known speeds. Earlier measurements using the OPS243-C module have reported measurements of the range of tripods and metal stands, as well as the speed of moving individuals and ceiling fans. These outputs are then corrected using a linear curve-fitting method [28]. In addition, signal processing software techniques are used to improve accuracy, including windowing (e.g., Hanning or Blackmann), peak detection with noise filtering, clutter suppression, and background subtraction.

In this work, an indoor application of the commercial radar module OPS243-C from OmniPreSense is presented, in which the range to stationary objects within a room measuring 4.88 × 3.91 m² is estimated in two scenarios. In the first scenario, objects are detected on individual walls and compared with their respective images, with linear fitting applied for accurate range detection. In the second scenario, the 24 GHz radar module is mounted on a rotating motor, and the ranges to objects within its 360° coverage are estimated. Next, a heatmap is plotted for object distance detection and further corrected using polynomial curve-fitting models based on root-mean-square errors (RMSEs) in MATLAB. The corrected 3D heatmap results, along with distance error corrections, are presented in the OPS243-C radar output data. Thus, the objective of this paper is to evaluate the accuracy range of the stationary object measurements obtained with the commercial radar module and to explore suitable methods for reducing distance measurement errors. Distance detection using error analysis and curve-fitting methods can be useful for other applications, such as monitoring elderly individuals' movement within a room or house, or tracking crop growth in agricultural fields.

II. DESCRIPTION AND WORKING OF OMNIPRESENSE MODULE OPS243-C

To scan stationary objects inside a room, a short-range radar module, OPS243-C, is utilized to provide their ranges at 24 GHz [29]. This module, OPS243-C, contains two sensors: an FMCW sensor and a Doppler sensor that report the range of stationary objects and the motion, speed, and direction of moving objects, respectively.

A. FMCW RADAR

The difference in frequency between the transmitted and corresponding received chirp signals serves as the basis for range estimation. The FMCW radar's reflected signal provides time-domain feedback, enabling it to determine the distances to stationary targets.

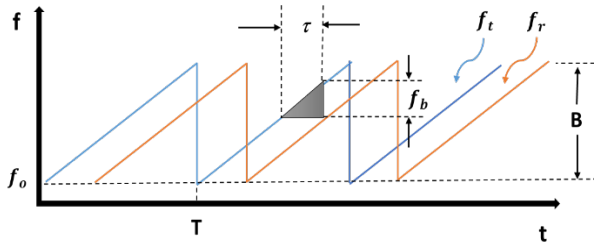

Figure 1. FMCW radar waveform.

Figure 1 shows that a linearly modulated continuous wave signal of frequency (f_t) is transmitted from the FMCW radar, which is also called the chirp signal. Consider $S_t(t)$ as the signal transmitted [30], which is given as

$$S_t(t) = A_{ot} \cos\left(2\pi f_o t + 2\pi \frac{B\,t^2}{T}\right) \quad (1)$$

where,
A_{ot} = Transmitted signal amplitude
f_o = Lowest frequency of the Radar system bandwidth
t = Time variable (in seconds)
B = Signal bandwidth $S_t(t)$
T = Period of the chirp signal

Tis he reflected signal $S_r(t)$ from the target is given as,

$$S_r(t) = A_o \cos\left((\pi f_o(t-\tau) + 2\pi \frac{B\ (t-\tau)^2}{T}\right) \quad (2)$$

where,

A_o = Amplitude of received signal

τ = Propagation delay that considers the distance between the target and the Radar and is given by $\tau = 2R/c$, R is the range of the target, c is the speed of light.

The transmitted signal frequency f_t can be expressed as[26],

$$f_t = f_o + \frac{df}{dt}t = f_o + \frac{2B}{T}t \quad (3)$$

The received signal frequency f_r can be expressed as follows.

$$f_r = f_o + \frac{df}{dt}(t-\tau) = f_o + \frac{2B}{T}(t-\tau) \quad (4)$$

The received signal displays a slightly different frequency than the transmitted signal due to the propagation delay, resulting in a beat frequency (f_b) , which is obtained after subtracting the transmitted frequency from the received frequency, and is given as,

$$f_b = f_t - f_r = \frac{2B\tau}{T} \quad (5)$$

Therefore, the range of the target R can be derived from:

$$f_b = f_t - f_r = \frac{2B\tau}{T} \quad (6)$$

This equation (6) is used by FMCW radar to obtain the range of objects without specifying the characteristics of objects.

B. Operating setup of OPS243-C

The operating setup of the radar module OPS243-C is depicted in Figure 2, where the TeraTerm or PuTTY interface of the module is used to extract the output in the form of speed or range, depending on the command provided. These command instructions are used to obtain the range of stationary objects, the speed of moving objects, and direction information. The main specifications of the OmniPreSense module OPS243-C are given in Table 1.

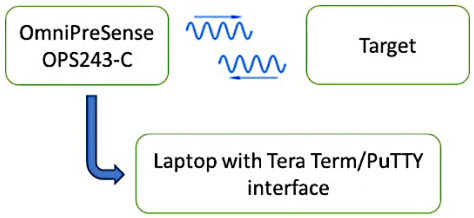

Figure 2. Operating setup of the OPS243-C RADAR module.

Table 1
Specification of OPS243-C

S.No	Specification	Value
1.	Frequency of operation	24GHz
2.	Range detection	Upto 100 m
3.	Speed detection	Upto 348 mph
4.	Direction reporting	Inbound/Outbound
5.	Industrial temp operation	-40 to +85°C
6.	Max Transmit Power	11dBm

III. EXPERIMENTAL SETUP

Two scenarios were developed: Scenario 1 - where the stationary OPS243-C recorded object information while pointing towards each wall for object detection inside a room; and Scenario 2 – where the OPS243-C recorded objects dynamically by rotating 360° in the same room using a rotating motor. As shown in the experimental workflow in Figure 3, the TeraTerm or PuTTY interface on the laptop captured the range FFT data by issuing the appropriate range command.

The captured range FFT (Fast Fourier Transform) data were in JSON format and saved in a .txt file, which was then imported into MATLAB. The MATLAB code processed the raw data in the log file, which contained FFT frames captured during multiple radar sweeps. The FFT values were then extracted and stored in a matrix representing radar return power across distance bins for each sweep. In the MATLAB code, RADAR parameters were set as FMCW sample size =512, Range FFT size = 1024, FMCW sample rate = 320kHz, and range resolution = 0.3123 m. A heatmap was plotted to observe the various scanned objects placed at different distances from the OPS243-C radar. To suppress background noise, a noise threshold was applied. A Gaussian smoothing filter was then applied to remove strong signals in the heatmap.

The object distance was detected at each sweep by multiplying the highest FFT value bin in each sweep by the range resolution. The object distances were then compared with the known distances, and heat maps confirmed deviations from the actual distances. Different polynomial curve-fitting models, i.e., 1st order, 2nd order, 3rd order, 4th order, 5th order, and 6th order, were applied and compared using RMSE to determine the best distance-measurement-error correction for the employed OPS243-C radar module. The predicted object distances were again compared with the actual distances and plotted in the 3D heatmap.

A. Scenario 1-Over Four Walls Individually

To obtain accurate predictions of object range or distance, each wall was scanned separately, and the output distances were fitted to achieve good predictions. The images of the radar acquiring data from each wall are shown in Figure 4. Details of the objects captured in the Scenario 1 are presented in Table 2.

Table 2
Actual and detected distances in the scanning of the objects in the room

S. No	Objects	Actual distances (meters)	Detected distances by OPS243-C RADAR (meters)		
			Scenario 1	Scenario 2	
1	Back wall	1.30	1.5	0°	1.5
2	Plastic chair	1.50	2.2	45°	2.2
3	Wooden almirah	1.72	2.5	90°	2.5
4	Steel almirah	2.48	2.8	135°	2.8
5	Bed	2.25	2.5	180°	2.5
6	Front wall (Diagonal corner)	3.87	3.7	225°	3.7
7	Sofa cum bed	2.02	-	-	1.5
8	Shoe stand	1.29	1.3	270°	1.3
9	Gate	2.13	3.1	315°	3.1

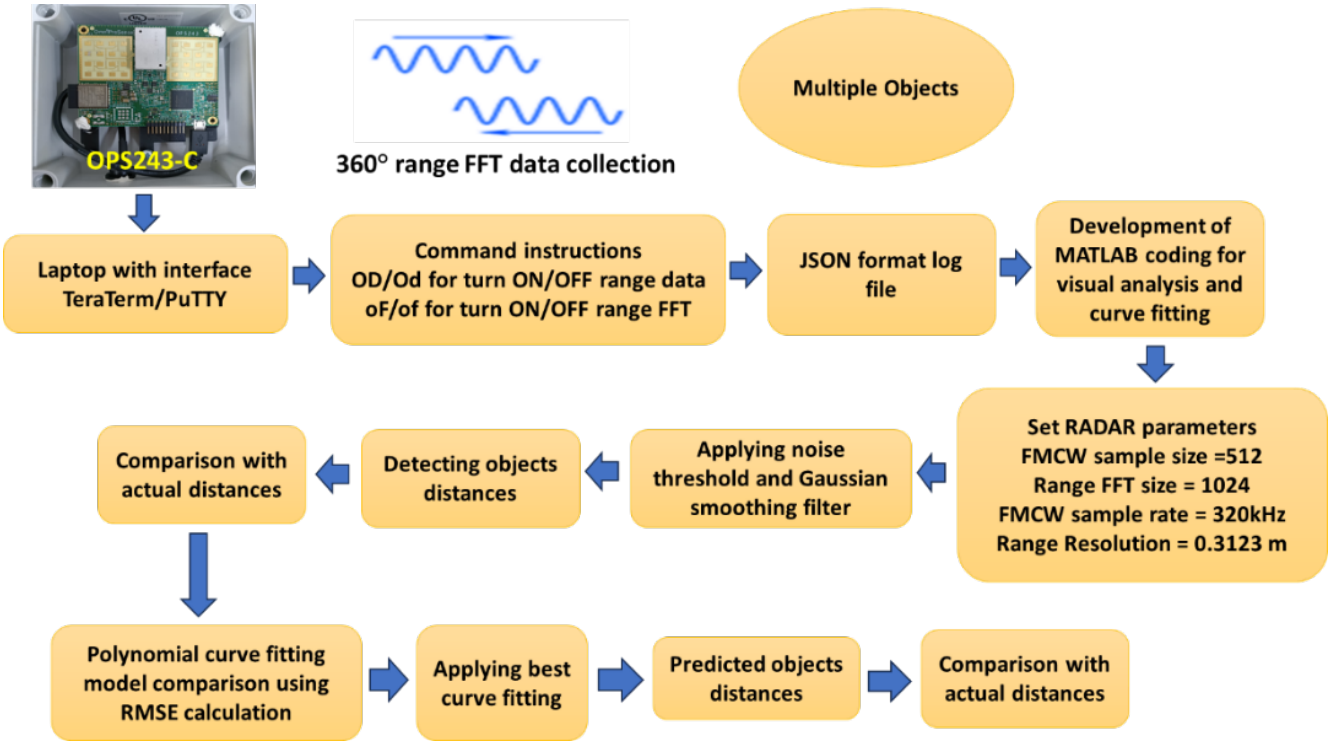

Figure 3. Workflow of data extraction and object detection, and prediction.

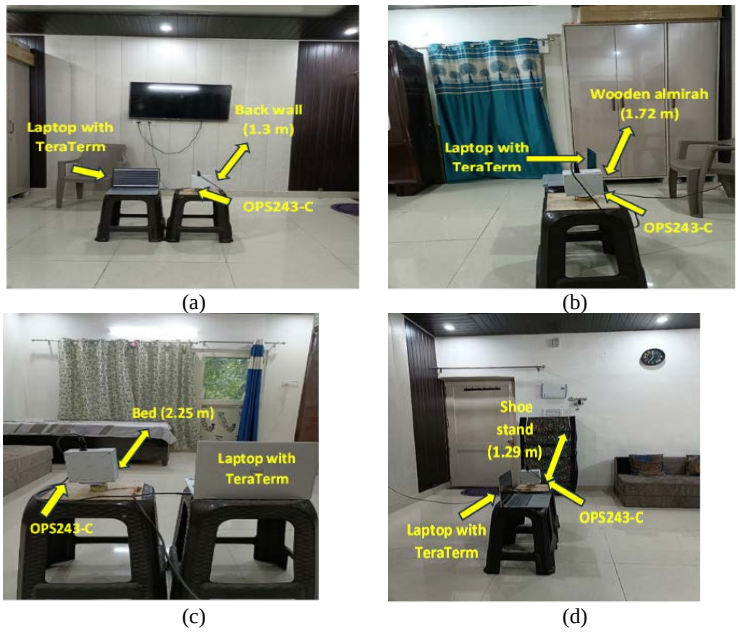

Figure 4. Different views of four walls for scanning application (a) Back wall, (b) Side wall 1, (c) Front wall, (d) Side wall 2.

B. Scenario 2-Over 360°

As depicted in Figure 5, the scanning of each object was performed over 360° in both clockwise and counterclockwise directions at approximately 24-second intervals, capturing the range FFT data using the TeraTerm interface on a laptop. As shown in Table 2, a significant difference was observed between actual and detected distances in both scenarios. Some objects were undetected in Scenario 1 due to the limited FoV, whereas in Scenario 2, non-linear differences between actual and detected distances were observed across different object types. Thus, different correction techniques were applied to the predicted object distances in Scenarios 1 and 2 to align them with the actual distances.

(c) (d)

Figure 5. Different views of four walls for scanning application (a) Back wall, (b) 135° angle view, (c) Front wall, (d) 315° angle view.

IV. RESULTS AND DISCUSSION

To predict the actual distance of all objects, single-side scanning was performed at multiple angles, as discussed for Scenario 1, and the results are shown in a heat map generated in MATLAB. As shown in Table 2, a linear fit was applied to predict more accurate data using MATLAB code. The suitable equations for each angle position of the objects from the radar were found as:

$y_{0^\circ} = 0.8325x$, $y_{45^\circ} = 0.6862x$, $y_{90^\circ} = 0.6884x$, $y_{135^\circ} = 0.8857x$, $y_{180^\circ} = 0.9006x$, $y_{225^\circ} = 1.0327x$, $y_{270^\circ} = 1.0327x$, and $y_{315^\circ} = 0.6820x$.

As mentioned earlier, to reduce the difference between the actual and detected distances as shown in Table 2, proper curve fitting was required for better prediction as the module captures noise and random fluctuations. Therefore, for closer fitting, the equations of 5th-order and 6th-order polynomial curve fitting were derived using MATLAB code and are given as:

$$y_{5th} = 2.5341x^5 + (-30.4986x^4) + 142.3546x^3 + (-321.2306x^2) + 350.1726x + (-146.1152) \quad (7)$$

$$y_{6th} = 1.9152x^6 + (-25.2257x^5) + 133.1084x^4 + (-358.7401x^3) + 518.6131x^2 + (-379.1107x) + 110.0762 \quad (8)$$

For each angle, Table 3 presents the radar module's detected distance, the predicted distance after fitting, and the corresponding image of objects at different angular positions in the room. Here, the dark red colour bar representing object positions at the corresponding angle for each wall confirms the actual distance and thus validates the applied fitting.

Figure 6(a) shows a heatmap of distance (m) vs. time (s) for continuous scanning of the entire room in 360° clockwise and anticlockwise directions, alternately. The repeated pattern in Figure 6(a) confirms that the module detected the same stationary objects in both clockwise and anticlockwise rotations, approximately every 24 seconds. The actual distances of the objects are indicated by the black dots in the heatmap, which are aligned with variations in red color intensity. Figure 6(b) shows a clean heatmap after applying a noise threshold of 20 dB below the maximum FFT amplitude and a Gaussian filter with a sigma value of 1. This led to spatial smoothing of the FFT data (over distance and time), reducing fluctuations and improving visual clarity in the heatmap.

Figure 6(c) presents comparisons of the actual distance, detected distance, and 5th- and 6th-order polynomial curve-fitting models, along with their corresponding RMSE values. This fitting parameter confirms that the 6th-order curve-fitting model, with an RMSE of 0.211, best fits the distance-measurement errors of the used OPS243-C radar.

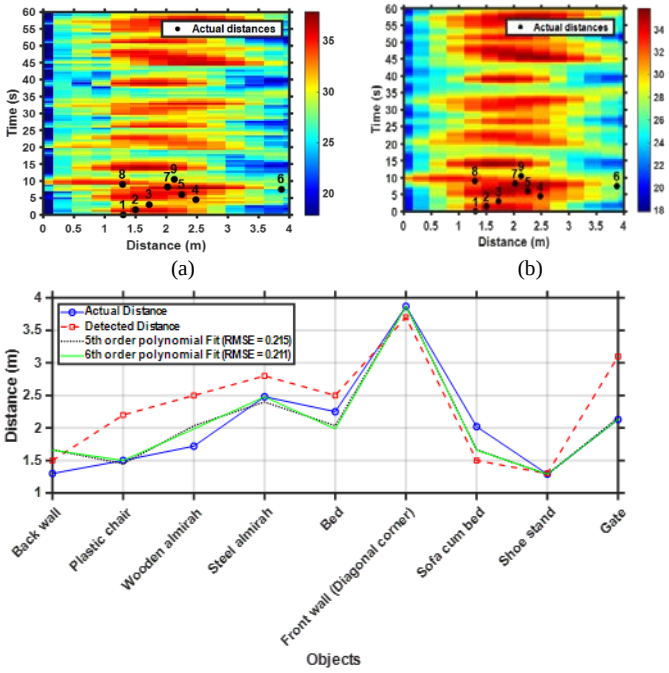

(a) (b) (c)

Figure 6. Heatmap and fit model comparison results from OPS243-C (a) radar raw data, (b) radar output after smoothing, (c) 5th-order and 6th-order polynomials curve fitting comparison

Table 3
Angle, Camera image, detected distance by RADAR module and predicted distance on scanning of the room

Angle and real distance	Images from the camera at different distances	Heatmap for distance detected by OPS243-C	Heatmap of predicted distance after curve fitting
0° (1.3 m)		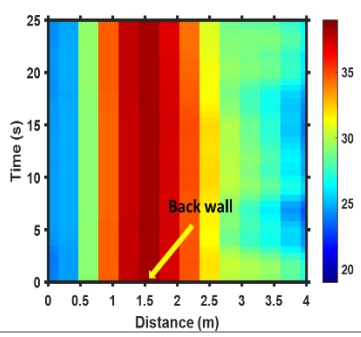	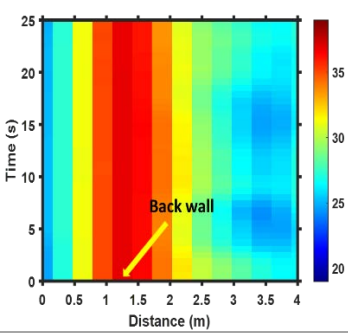

45°
(1.5 m)

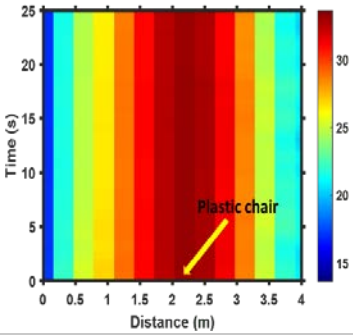

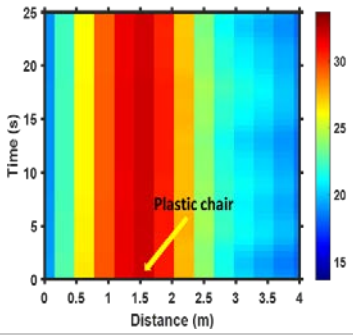

90°
(1.72 m)

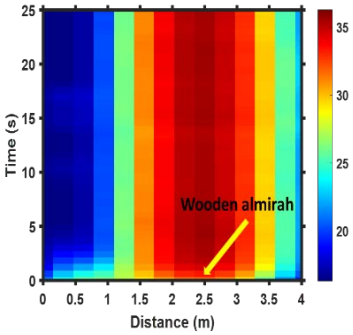

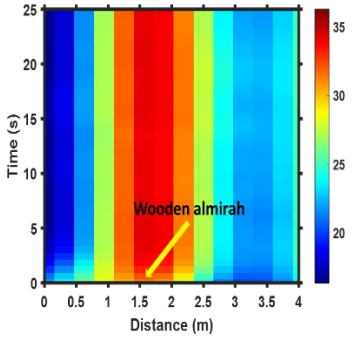

135°
(2.48 m)

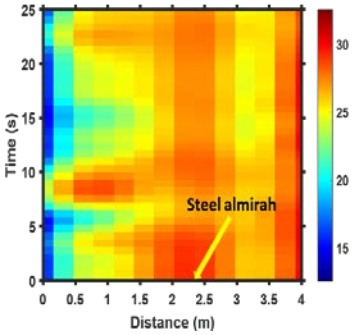

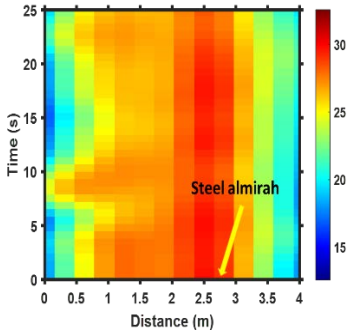

180°
(2.25 m)

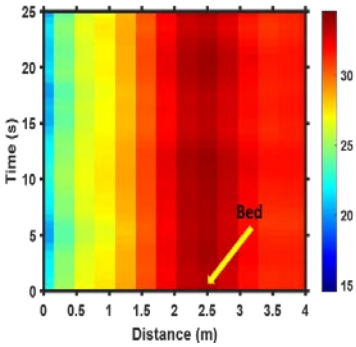

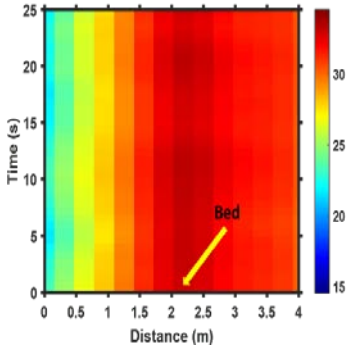

225°
(3.87 m)

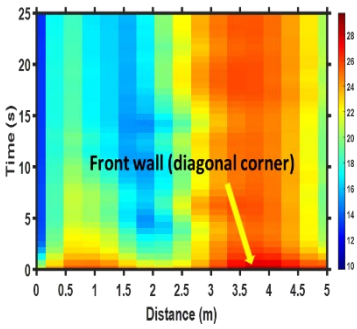

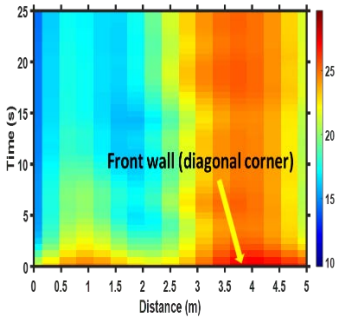

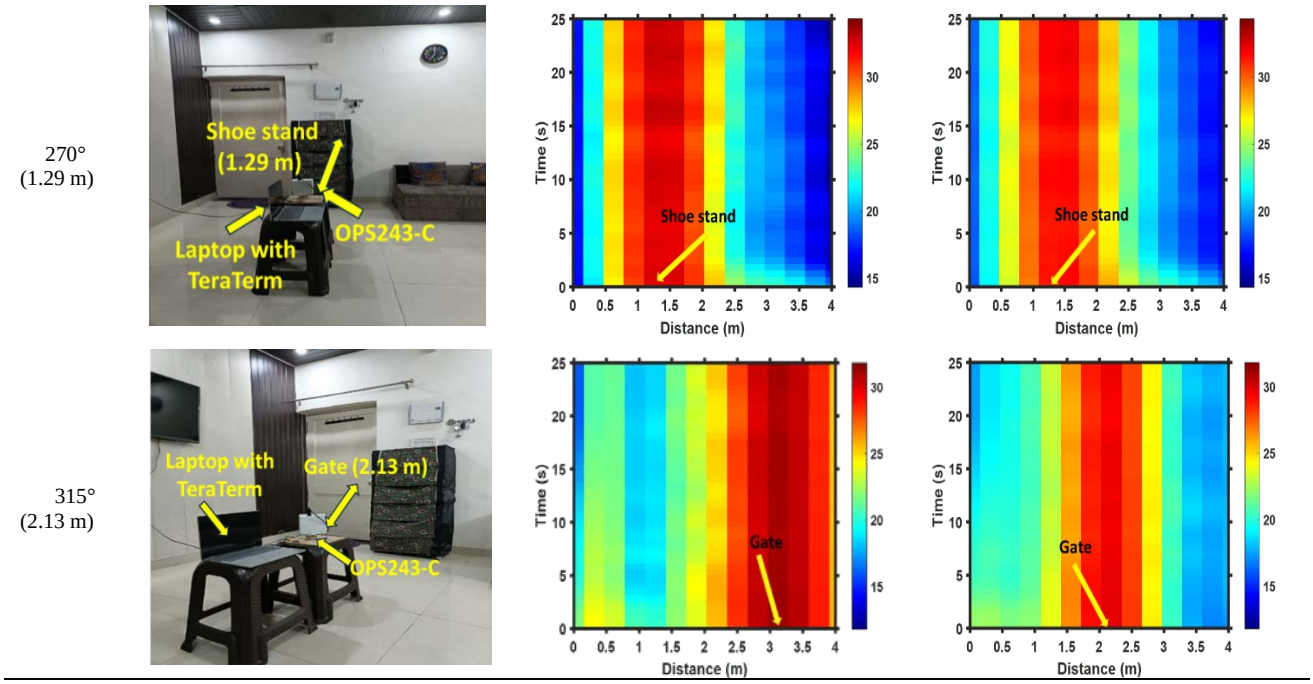

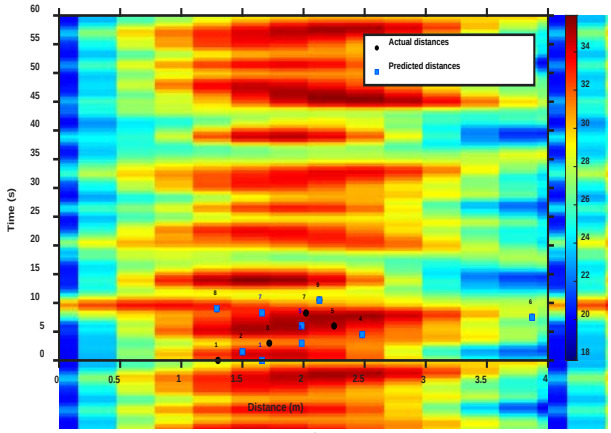

`(a)

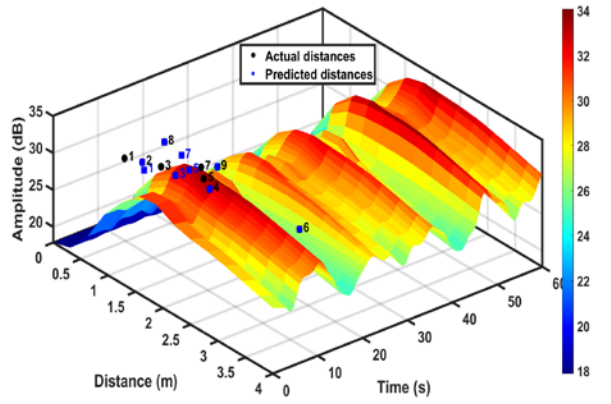

(b)

Figure 7(a) Actual vs Predicted distance 2D heatmap with 6th-order polynomial curve fitting (b) 3D view of Actual vs Predicted distance heatmap with 6th degree polynomial curve fitting.

Figure 7(a) shows a 2D heatmap of the complete room scan after applying the 6th-order curve-fitting model, including both actual and predicted distances. Here, most of the objects, such as a plastic chair, a steel almirah, the front wall (diagonal corner), a shoe stand, and a gate, depicted in blue color squares, show overlap between the predicted and actual distances. Some objects, such as the back wall, sofa cum bed, wooden almirah, and the bed represented in black dots, indicate that the predicted distances are close to the actual distance after applying the curve-fitting method. This difference is due to the disparate material compositions of these objects. However, it also confirms that the proposed fitting model was best suited for this application. Figure 7(b) shows a 3D view of the predicted and actual distances for effective visualization, further validating the proper scanning of all objects in a 360° view by the utilized radar module.

Table 4 compares existing techniques with the proposed radar-heatmap-based calibration method for indoor scanning applications. In [15], the approach relies on CFAR-based detection, clustering, and multi-target tracking algorithms to estimate the number of people in crowded environments. While such methods demonstrate effective tracking of moving targets, they primarily focus on human activity monitoring and involve relatively complex processing. In [16], a CNN-based framework was proposed for device-free human localization and posture sensing using range–angle radar maps. Such approaches achieve good localization performance; however, they require large labelled datasets and significant computational resources for training. In [17], seamless passive tracking using mmWave radar focuses on tracking moving targets in LOS and NLOS environments, leveraging multipath modelling and tracking algorithms. In [18], the proposed mmWave dual-mode radar sensor uses the long-range and high-resolution radar modes and utilizes RANSAC-based line detection to estimate wall structures for indoor environment mapping. However, this system relies on specialized radar hardware and robotic motion to accumulate mapping data.

Table 4

Comparison Table with Previous techniques for Indoor scanning

Study	Radar Type	Frequency	Application	Technique	Limitation
[12]	Doppler	-	Velocity estimation of static and moving objects	Deep neural network architecture	dependence on large training datasets
[15]	MIMO FMCW	24 GHz	Counting people	wavelet decomposition+ clustering + tracking	Focus on moving targets
[16]	FMCW	24 GHz	Human localization	CNN deep Learning	Requires training data
[17]	FMCW	77 GHz	NLOS/LOS tracking	Neural network architecture	High complexity
[18]	MIMO FMCW	62 GHz	Indoor environment mapping.	2D range map	High complexity
This work	FMCW and Doppler	24 GHz	Indoor environment scanning	Heatmap analysis + Calibration	Low complexity

In contrast, the proposed method in this work focused on indoor environment scanning and on improving distance estimation accuracy through radar heatmap visualization. This approach provided a computationally efficient framework that does not require complex target-tracking algorithms. Therefore, it provided a simpler and more computationally efficient approach for indoor scanning applications. As seen in Table 4, the heatmap was evaluated directly from the radar data with and without curve fitting; the visualization of objects was easier than the complex evaluation techniques by previous researchers, summarized in Table 4.

V. CONCLUSION

In this paper, the scanning results for various objects in a typical room were presented, with the FMCW radar and the OmniPreSense OPS243-C module at 24 GHz being used to measure the distances to objects placed randomly. The predicted distances of objects were presented as a heatmap after correcting the detected distances in two scenarios: over each wall and over clockwise and anticlockwise rotations of 360 °. It was observed that objects made of different materials were detected with varying error ranges; therefore, linear curve fitting was applied for each wall scan, while polynomial curve fitting was applied for the entire room scan. The predicted distances were obtained using a 6th-order polynomial curve-fitting model generated by another MATLAB code, selected based on a minimum RMSE of 0.211. The distance results were further validated by capturing radar data towards each wall of the room and comparing them with their corresponding real-time images. This approach can be further extended to simultaneously detect stationary objects, such as crops in an agricultural field, for health monitoring.

ACKNOWLEDGMENT

The authors would like to acknowledge funding support, in part, from Visvesvaraya Ph.D. Fellowship Scheme, Phase II from the Ministry of Electronics & Information Technology (MeitY), Government of India and University of Delhi for IoE Grant No.: IoE/ 2021/12/FRP dated 31-08-2022.

CONFLICT OF INTEREST

Authors declare that there is no conflict of interests regarding the publication of the paper.

AUTHOR CONTRIBUTION

The authors confirm contribution to the paper as follows: study conception and design: Shalini Kashyap, Amit Birwal, Kamlesh Patel; data collection: Shalini Kashyap; analysis and interpretation of findings: Shalini Kashyap, Amit Birwal, Kamlesh Patel; draft manuscript preparation: Shalini Kashyap, Kamlesh Patel. All authors had reviewed the findings and approved the final manuscript.

REFERENCES

[1] Yılmaz, H. Ö., & Yaman, F., "Metamaterial antenna designs for a 5.8-GHz Doppler radar," IEEE Transactions on Instrumentation and Measurement, vol. 69, no. 4, pp. 1775-1782., 2019.

[2] Kathuria, N., & Seet, B. C., "24 ghz flexible antenna for doppler radar-based human vital signs monitoring," Sensors, vol. 21, no. 11, p. 3737, 2021.

[3] Ridhia, F., Pramudita, A. A., & Suratman, F. Y., "Soil Water Content Estimation over Plantation Area Using FMCW Radar," Progress In Electromagnetics Research B, vol. 101, pp. 155-173, 2023.

[4] Lim, H. S., Park, H. M., Lee, J. E., Kim, Y. H., & Lee, S., "Lane-by-lane traffic monitoring using 24.1 GHz FMCW radar system," IEEE Access, vol. 9, pp. 14677-14687, 2021.

[5] Hoog, N. A., van den Berg, T. E., & Bindra, H. S., "A 60 GHz pulsed coherent radar for online monitoring of the withering condition of leave," Sensors and Actuators A: Physical, vol. 343, p. 113693., 2022.

[6] Y. Li, C. Gu and J. Mao, "An In-Vehicle Occupant Detection Technique Based on a 60 GHz FMCW MIMO Radar," in IEEE MTT-S International Wireless Symposium (IWS), Harbin, China,, 2022.

[7] ADAS, Detection and Simple Tracking Method for, "Detection and Simple Tracking Method for ADAS using a mmWave Radar," in IEEE 4th Annual Flagship India Council International Subsections Conference (INDISCON),, Mysore, India, 2023.

[8] Wahyu, Y., Yanti, R. J., Prasetya, S., Wicaksana, B. B. S., Sukoco, B. E., Ridhia, F., & Pramudita, A. A, "24 GHz FMCW Radar for Non-Contact Respiratory Detection," in 2022 6th International Conference on Information Technology, Information Systems and Electrical Engineering (ICITISEE), Yogyakarta, Indonesia, 2022.

[9] Prasetya, Suisbiyanto, et al, "Data Analyzes and conversion of Patient's Respiratory FMCW Radar to the Internet of Things," in 2023 International Seminar on Intelligent Technology and Its Applications (ISITIA), 2023.

[10] Pramudita, A. A., Lin, D. B., Hsieh, S. N., Ali, E., Ryanu, H. H., Adiprabowo, T., & Purnomo, A. T., "Radar System for Detecting Respiration Vital Sign of Live Victim Behind the Wall," IEEE Sensors Journal, vol. 22, no. 15, pp. 14670-14685, 2022.

[11] Elishiah Miller, Nilanjan Banerjee, Ting Zhu, "Smart homes that detect sneeze, cough, and face touching," Smart health, vol. 19, p. 100170, 2021.

[12] Schwan, J., Dhamija, A., & Boult, T., "I-MOVE: Independent Moving Objects for Velocity Estimation," in Proceedings of the IEEE/CVF Winter Conference on Applications of Computer Vision, 2020.

[13] Miller, E., MacFarlane, Z., Martin, S., Banerjee, N., & Zhu, T., "Radar-based monitoring system for medication tampering using data augmentation and multivariate time series classification," smart health, vol. 23, pp. 2352-6483, 2022.

[14] Ramadhamy, Q. H., Pramudita, A. A., & Suratman, F. Y., "Clutter Reduction in Detecting Trapped Human Respiration under Rubble for FMCW Radar System," in 2023 International Seminar on Intelligent Technology and Its Applications (ISITIA), 2023.
[15] D. Wang, S. Yuan, A. Yarovoy and F. Fioranelli, "Grouped Target Tracking and Seamless People Counting With a 24-GHz MIMO FMCW," IEEE Transactions on Radar Systems, vol. 3, pp. 1298-1308, 2025.
[16] S. Yang and Y. Kim, "Single 24-GHz FMCW Radar-Based Indoor Device-Free Human Localization and Posture Sensing With CNN," IEEE Sensors Journal, vol. 23, no. 3, pp. 3059-3068, 2023.
[17] Z. Li, X. Xia, Z. Chen and A. Bi, "Seamless Passive Tracking Based on mmWave Radar in Indoor NLOS/LOS Environments," IEEE Transactions on Industrial Informatics, vol. 21, no. 10, pp. 8176-8185, 2025.
[18] Lee, S.; Kwon, S.-Y.; Kim, B.-J.; Lim, H.-S.; Lee, J.-E. , "Dual-Mode Radar Sensor for Indoor Environment Mapping," Sensors, vol. 21, p. 2469, 2021.
[19] G. Gennarelli, C. Noviello, G. Ludeno, G. Esposito, F. Soldovieri and I. Catapano, "24 GHz FMCW MIMO Radar for Marine Target Localization: A Feasibility Study," IEEE Access, vol. 10, pp. 68240-68256, 2022.
[20] K. Byeon, B. J. Seo, D. Park, G. Jung, W. Jang and Y. S. Eo, "A 24 GHz Antenna Embedded Radar Sensor Using UWB Radar SoC," in 2022 Asia-Pacific Microwave Conference (APMC), Yokohama, Japan, 2022.
[21] R. Vincenti Gatti, G. Cicioni, A. Spigarelli, G. Orecchini, C. Saltalippi and F. Alimenti, "A Dual-Mode FMCW-Doppler Radar With a Frequency Scanning Antenna for River Imaging Applications," IEEE Access, vol. 12, pp. 86132-86143, 2024.
[22] E. Tavanti, A. Rizik, A. Fedeli, D. D. Caviglia and A. Randazzo, "A Short-Range FMCW Radar-Based Approach for Multi-Target Human-Vehicle Detection," IEEE Transactions on Geoscience and Remote Sensing, vol. 60, pp. 1-16, 2022.
[23] Xu, Z. Zhu and F., "Demonstration of 3-D Security Imaging at 24 GHz With a 1-D Sparse MIMO Array," IEEE Geoscience and Remote Sensing Letters, vol. 17, no. 12, pp. 2090-2094, 2020.
[24] J. He, S. Terashima, H. Yamada and S. Kidera, "Diffraction Signal-Based Human Recognition in Non-Line-of-Sight (NLOS) Situation for Millimeter Wave Radar," IEEE Journal of Selected Topics in Applied Earth Observations and Remote Sensing, vol. 14, pp. 4370-4380, 2021.
[25] M. Abdelhamid, A. Safa, L. Ismail and A. Mohamed, "FMCW Radar for Human Detection in Collapsed Structures for Post-Disaster Search and Rescue," in 2025 International Wireless Communications and Mobile Computing (IWCMC), Abu Dhabi, United Arab Emirates, 2025.
[26] H. -C. Chang, C. -K. Chen, C. -W. Cho, S. -A. Yu and C. -T. M. Wu, "Integrated Single-Board 24 GHz FMCW Radar and Infrared Thermal Sensor Fusion for Target Detection," in 2025 IEEE MTT-S International Microwave Biomedical Conference (IMBioC), Kaohsiung, Taiwan, 2025.
[27] V. R. Z. Iskandar, B. Prasetya and A. A. Pramudita, "Vegetation Density Profiling Using FMCW Radar for Plant Population Estimation," in 2024 12th Electrical Power, Electronics, Communications, Controls and Informatics Seminar (EECCIS), Malang, Indonesia, 2024.
[28] Kashyap, S., Birwal, A., & Patel, K, "Extraction of Range and Speed data from A 24 GHz Radar Module," in 2024 International Conference on Integrated Circuits, Communication, and Computing Systems (ICIC3S), Una, Himachal Pradesh, India, 2024.
[29] "OmniPreSense," [Online]. Available: https://omnipresense.com.
[30] Kim, S. Yang and Y., "Single 24-GHz FMCW Radar-Based Indoor Device-Free Human Localization and Posture Sensing With CNN," IEEE Sensors Journal, vol. 23, no. 3, pp. 3059-3068, 2023.